PROCEEDINGS OF SPIE

SPIEDigitalLibrary.org/conference-proceedings-of-spie

High-performance optical modulators based on stepped quantum wells

Mohseni, H., Chan, W., An, H., Ulmer, A., Capewell, D.

H. Mohseni, W. K. Chan, H. An, A. Ulmer, D. Capewell, "High-performance optical modulators based on stepped quantum wells," Proc. SPIE 6127, Quantum Sensing and Nanophotonic Devices III, 61270D (28 February 2006); doi: 10.1117/12.640530

SPIE.

Event: Integrated Optoelectronic Devices 2006, 2006, San Jose, California, United States

Downloaded From: https://www.spiedigitallibrary.org/conference-proceedings-of-spie on 14 Sep 2021 Terms of Use: https://www.spiedigitallibrary.org/terms-of-use

High-Performance Optical Modulators Based on Stepped Quantum Wells

H. Mohseni
Department of Electrical and Computer Engineering, Northwestern University
Evanston, IL 60208; e-mail: hmohseni@ece.northwestern.edu

W. K. Chan, H. An, A. Ulmer, and D. Capewell
Sarnoff Corporation, 201 Washington Road, Princeton NJ 08543

Abstract: High-speed and high-performance optical phase and amplitude modulators are critical components of many photonic systems. Semiconductor-based modulators are very attractive, since they can be monolithically integrated with other semiconductor devices. Unfortunately, the commonly used modulators based on square quantum wells have inherent properties that limit their modulation performance.
We present a new class of quantum wells called "stepped quantum wells" (SQW) with extra degrees of freedom that can be used to design high performance optical modulators. We demonstrated SQW phase modulators with nearly one order of magnitude higher efficiency than their counterparts. Also, linearized modulators based on SQW with more than two orders of magnitude higher linearity than the existing semiconductor modulators are presented. Finally, high-performance surface-normal modulators based on SQWs with nearly two times better efficiency and 7 dB higher extinction ratio compared with the conventional devices with rectangular and coupled-quantum well active layers are demonstrated.

I. Introduction

Optical modulators are adding the analog or digital data to the optical carrier, and hence are occasionally the "interface" between the electronic and photonic worlds. Moreover they can be used to manipulate light in the time-space domain and change the temporal[1] and spatial[2] properties of light. Therefore, optical modulators are enabling technologies that can affect the performance of a wide range of systems. Although lithium niobate based optical modulators are the backbones of many optical systems, they cannot be integrated and require rather large operating voltages. Therefore, there have been extensive efforts to enhance the electrooptic coefficient with a low optical absorption in the III-V material. The most promising structures are symmetric[3] and asymmetric[4] coupled quantum wells, with theoretical enhancements approaching a factor of ten[4]. Experimentally, a factor of five higher electrorefraction has been obtained in an AlGaAs/GaAs asymmetric coupled quantum well[5]. However, similar improvements have not been demonstrated in the InP-based materials. We have conceived a novel class of quantum wells with potential steps inside the main wells. Our theoretical and experimental

Quantum Sensing and Nanophotonic Devices III, edited by Manijeh Razeghi, Gail J. Brown,
Proc. of SPIE Vol. 6127, 61270D, (2006) · 0277-786X/06/$15 · doi: 10.1117/12.640530

Downloaded From: https://www.spiedigitallibrary.org/conference-proceedings-of-spie on 14 Sep 2021
Terms of Use: https://www.spiedigitallibrary.org/terms-of-use

results show that these so-called "stepped quantum wells" have superior properties compared to the conventional quantum wells[6,7] and even advanced coupled quantum wells[8]. In the following we shall present some of the unique properties of the stepped quantum wells for three applications: high sensitivity phase modulators, high linearity phase modulators, and surface-normal amplitude modulators.

II. Modeling

We developed a modeling and simulation software package for semiconductor-based optical modulators. Figure 1 shows the software interface with calculated electron, heavy, and light-hole wavefunctions for a given set of material composition and thickness. The optical absorption spectrum of the quantum well was then calculated using an effective mass approach. The excitonic effect was calculated based on a variational method[9]. The electric field inside the active region was calculated using diffusion-drift and Poisson equations.

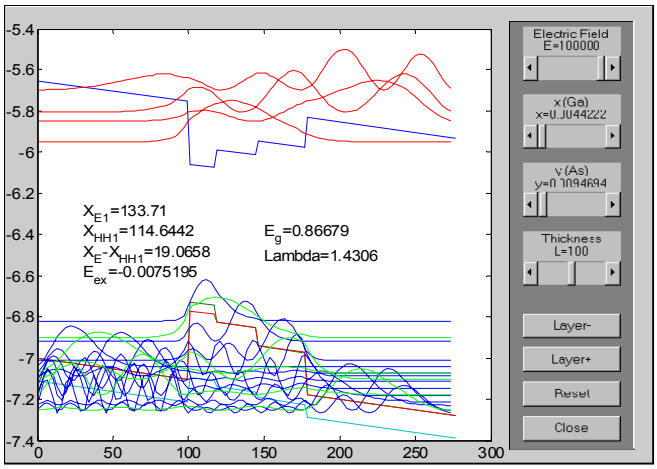

Figure 1. A snapshot of the simulation software.

Optical absorption coefficient versus the applied bias to the device was calculated from the electric field and applied voltage relationship, combined with the optical absorption and applied field relationship. Change of index in the material was then calculated using the Kramers-Kronig relation. We found excellent agreement between our theoretical and experimental data for many different devices and applications (see Figure 2)

Downloaded From: https://www.spiedigitallibrary.org/conference-proceedings-of-spie on 14 Sep 2021
Terms of Use: https://www.spiedigitallibrary.org/terms-of-use

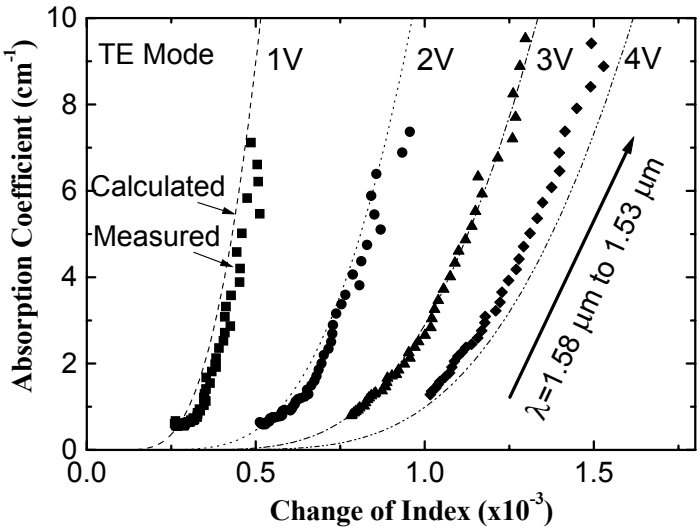

Figure 2. Calculated and measured optical absorption coefficient and change of index versus applied bias.

III. General Modulator Implementation

Different modulator structures are based on GaInAsP/AlInAs material grown by low-pressure metal organic vapor phase epitaxy (MOVPE) on n-type InP substrates. Active layers were multiple layers of stepped quantum wells. We used strained layers that were balanced for some applications where the simulation indicated as optimum designs. The materials were processed into long mesa-type modulators for edge coupled phase modulators, and circular mesas for surface-normal devices (see Figure 3)

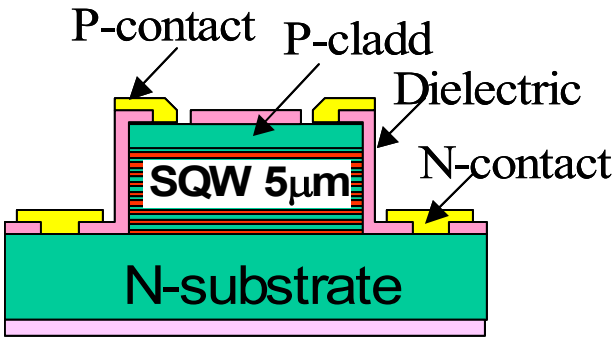

Figure 3. Schematic of the processed device.

IV. Measurement and Results

Highly Efficient Phase Modulators

We measured optical absorption coefficient and change of index of the optimized modulators by measuring Fabry-Perot oscillation, optical transmission, and the modulator

Downloaded From: https://www.spiedigitallibrary.org/conference-proceedings-of-spie on 14 Sep 2021
Terms of Use: https://www.spiedigitallibrary.org/terms-of-use

photoresponse. Leakage currents were significantly lower than values that could cause heat-induced change of index. Figure 2 compares the measured and calculated optical absorption coefficient versus change of index for a modulator with 3SQW active region. The data points are collected from λ=1.53 μm to 1.58 μm with 10 nm increments, and for bias values of one to four volts. Calculated change of index and optical absorption coefficient show good agreement to the measured data for bias values up to nearly three volts. We believe that field-dependent excitonic broadening is the main reason for the gradual deviation between the measured and modeled data at higher bias values. We compared the performance of 3SQW and RQW systematically. Since the detuning from the energy gap of the devices has a significant effect on the measurement, we only compared devices with similar bandgap energies. Also, plotting α versus Δn/ΔV, and eliminating their wavelength dependency reduced the detuning effect in our comparison. Figure 4 compares the performance of a modulator with 3SQW active region to a modulator with a conventional RQW at λ=1.550 μm and TE polarization. The layer thickness and composition of the RQW were optimized for maximum Δn/ΔV using our modeling approach.

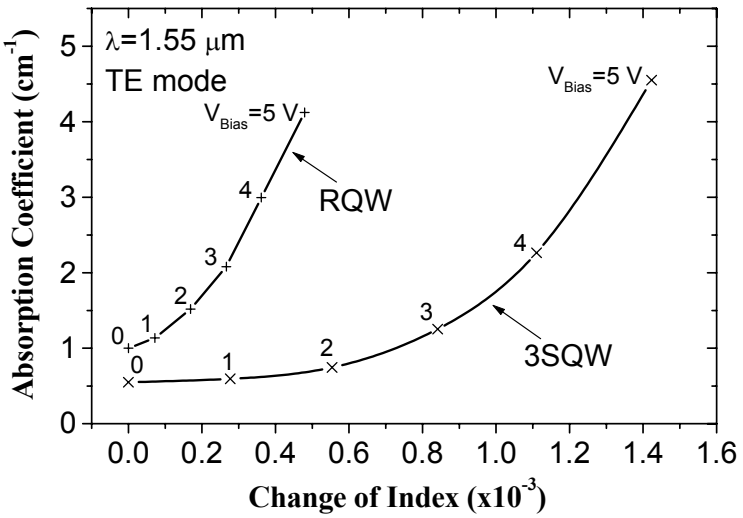

Figure 4. Performance of a modulator with 3SQW active region compared to a modulator with a conventional RQW active region at λ=1.550 μm and TE polarization.

The barrier of the RQW is InP (85 Å) and the quantum well is $In_{0.58}Ga_{0.42}As_{0.90}P_{0.10}$ (85 Å). The peak photoluminescence energies of the 3SQW and RQW were 0.877 eV and 0.875 eV respectively. Variation in the growth quality was negligible, since the samples were a few growth run apart. The measured change of index of the RQW at $\alpha \sim 1\ cm^{-1}$ is about 1×10^{-4}/V, similar to the reported values in the literature[10], while it is about 2.8×10^{-4}/V for 3SQW. Also, note that both α and $\Delta\alpha/\Delta V$ are smaller in the 3SQW for bias values below ~4 Volts. The importance of a low optical loss can be better understood by considering the gain of an impedance matched analog RF photonic link[11]:

Downloaded From: https://www.spiedigitallibrary.org/conference-proceedings-of-spie on 14 Sep 2021
Terms of Use: https://www.spiedigitallibrary.org/terms-of-use

$$G = \left(\frac{e^{-\alpha L}}{V_\pi} \cdot \frac{\pi 10^{-l/10} R r_d P}{4} \right)^2 \quad \text{Equation 1}$$

where α is the optical absorption coefficient, L is the length of the modulator, and V_π is the voltage required for a π phase shift, R is the detector responsivity, r_d is the detector resistance, P is the laser power, and l is the total loss from the interconnects and fiber optics in decibel. Retaining the relevant parameter to the modulator, one can define modulator figure of merit as $M=(\exp(-\alpha L)/V_\pi)^2$. Assuming a small change of index, the value of V_π can be calculated as $V_\pi=\lambda/[2L(\Delta n/\Delta V)]$. Here λ is the laser wavelength and $\Delta n/\Delta V$ is the change of index versus change of bias in the modulator. Therefore, the optimum length of the modulator required to maximize M can be calculated as $L_{opt}=1/\alpha$ and the figure of merit of a modulator with the optimum length becomes:

$$M_{opt} = 4e^{-2}\left(\frac{\Delta n/\Delta V}{\alpha\lambda} \right)^2 \quad \text{Equation 2}$$

Inserting the measured values of optical absorption coefficient and change of index for bias values of 2 volts into Eq. 2, one obtains M_{opt}~0.10 V^{-2} for the RQW and M_{opt}~3.60 V^{-2} for 3SQW. This means that replacing the conventional RQW with the 3SQW can improve the gain of an analog RF link by 15.5 dB. Low electroabsorption is also crucial for other applications such as resonant-enhanced micro-ring modulators[12], where the ring quality factor Q is inversely proportional to the absorption coefficient α. Another important parameter for an electrorefractive modulator is a high chirp factor $\Delta n/\Delta k=(4\pi/\lambda)(\Delta n/\Delta\alpha)$, since it ensures a high contrast ratio in Mach-Zehnder (MZ) modulators[13]. Figure 4 illustrates the measured chirp factor of modulators with 3SQW and RQW active regions at different bias values. The higher value of chirp in the 3SQW is due to both a higher change of index and lower change of absorption.

Highly Linear Phase Modulators

Highly linear optical phase modulators are attractive for many applications including laser gyroscopes, multi-wavelength laser sources, beam steering, and photonic arbitrary waveform generators. Although commonly used phase modulators based on lithium niobate have an inherent high linearity, they cannot provide the degree of integration required for applications such as high-speed optical NxN switches[2], where hundreds of closely spaced modulators are needed. In contrast, semiconductor based phase modulators can provide a high degree of integration, but they are inherently non-linear. The main sources of non-linearity in the semiconductor phase modulators are quadratic electrooptic (QEO) effect. Although using bulk semiconductor, instead of quantum well, active layers can reduce these effects, it would also reduce the modulation efficiency significantly. We utilized stepped quantum wells to make efficient linearized phase modulators. Modulator linearity is more than one order of magnitude higher than bulk GaAs and GaInAsP, while modulation efficiency is comparable to the best low-loss quantum well modulators.

Thickness and composition of the quantum well layers were optimized for high linearity, while keeping the absorption coefficient below ~1 cm^{-1}. Modulator structures are

Downloaded From: https://www.spiedigitallibrary.org/conference-proceedings-of-spie on 14 Sep 2021
Terms of Use: https://www.spiedigitallibrary.org/terms-of-use

grown by low-pressure metal organic vapor phase epitaxy (MOVPE) on n-type InP substrates. The doping profile in the cladding layer was designed to further improve the phase linearity. Conventional phase modulators with square quantum well active layers where also grown as references. The material was then processed into shallow etched waveguides for optical and electrical measurements.

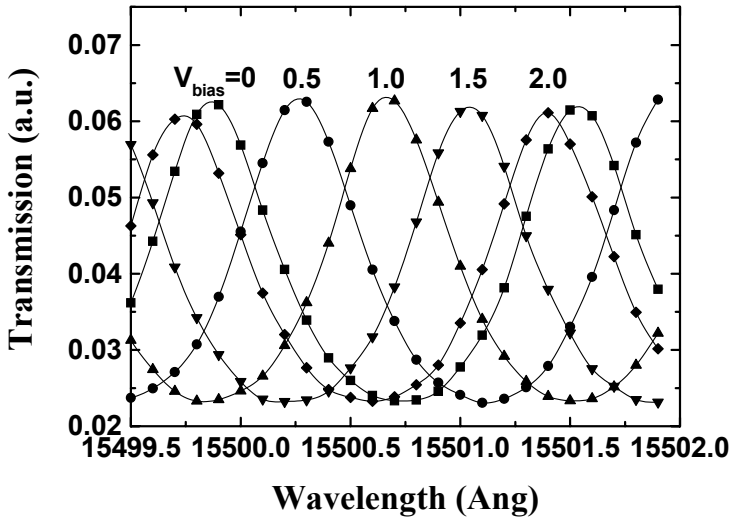

Figure 5 Fabry-Perot oscillation shift in a 2 mm long phase modulator for different bias values.

Optical absorption coefficient and change of index of the modulators are measured using Fabry-Perot oscillation shifts. Figure 5 shows an example of the measured Fabry-Perot oscillation shift in a 2 mm long modulator versus the modulator bias at λ~1550 nm. Figure 6 shows the measured change of index versus the applied reverse bias at different wavelengths for a linearized phase modulator.

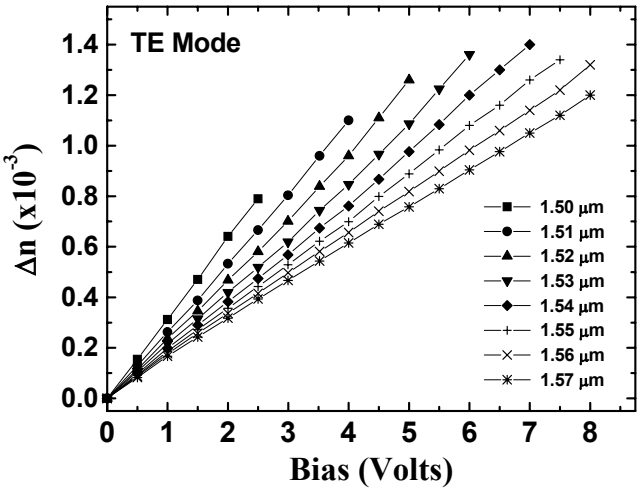

Figure 6 Measured change of index versus reverse bias voltage at different wavelengths

Downloaded From: https://www.spiedigitallibrary.org/conference-proceedings-of-spie on 14 Sep 2021
Terms of Use: https://www.spiedigitallibrary.org/terms-of-use

Change of index versus bias is linear over the measured wavelength range of 1500 to 1570 nm. In order to compare the quadratic and linear electrooptic effects, we fit a second order polynomial $\Delta n=A_0+A_1V+A_2V^2$ to the measured data points, and use A_1/A_2 ratio as a measure of linearity. Figure 7 compares the change of index versus bias of a linearized modulator to a conventional modulator at λ=1560 nm for TE polarization. Linearized modulator shows A_1/A_2 ratio of ~640, while the modulator with a conventional design shows A_1/A_2 ratio of ~10. The linearized modulator shows higher linearity than the modulators based on bulk semiconductors. For instance, calculated A_1/A_2 ratio for GaAs and InP at λ~1550 nm is about 75 and 20 respectively[14]. The modulation efficiency of the linearized modulator is about 48°/mm.V with a maximum loss of ~1 cm^{-1}, which is more than three times better than the efficiency of bulk-based modulators[14].

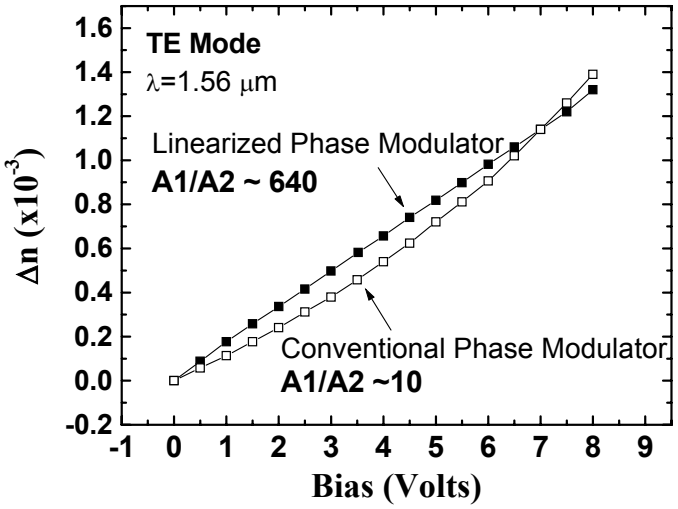

Figure 7 change of index versus bias for a linearized phase modulator compared to a conventional phase modulator at λ=1.56 μm and for TE polarization.

Highly Efficient Surface-normal Amplitude Modulators

Surface-normal optical modulators are attractive devices for applications in free-space photonic link between mobile platforms[15] as well as for optical interconnects[16]. Although several surface-normal modulator technologies are available, p-i-n quantum well based modulators are the most attractive of these because they operate at the highest frequency and over the widest temperature range. Nevertheless, these devices still suffer from high power consumption, limited data bandwidth, and limited optical bandwidth. Reducing the device area can directly improve the power consumption and data bandwidth, since the former is inversely and the latter is directly proportional to the device area. Unfortunately, reducing the device area can significantly degrade the link performance, since the gain of a photonic link based on a retroreflector is proportional to the fourth

Downloaded From: https://www.spiedigitallibrary.org/conference-proceedings-of-spie on 14 Sep 2021
Terms of Use: https://www.spiedigitallibrary.org/terms-of-use

power of the modulator area[15]. Recently, coupled quantum wells have been used to reduce the operating voltage, and hence the power consumption, of the modulator[17]. However, the data bandwidth of these devices is still limited by RC to about 15 MHz, and the optical bandwidth is only about 10 nm. Low optical bandwidth is particularly unfavorable, since the change of modulator temperature can change the modulator bandgap and hence reduce the modulation depth significantly. Consequently, a low optical bandwidth leads to significantly higher system power consumption, cost, and volume due to the need for temperature control.

High leakage current and premature breakdown are the most important source of low yield for large area modulators. We used a dielectric based passivation method to reduce the surface leakage current (see Figure 3). Figure 8 shows excellent current-voltage characteristics of a modulator with 5.1 mm diameter at zero illumination at room temperature. The dark current of the device is ~10 μA at –95 volts, which is equal to a current density of ~50 μA/cm^2 at an electric field of ~190kV/cm. This is similar to the lowest leakage current density of modulators based on InGaAs/GaAs multi-quantum wells with a much wider bandgap and at a similar electric field[18]. Also, the device shows a current that is proportional to the square root of voltage up to -80 volts. Therefore, the leakage is generation-recombination limited up to a very high voltage at room temperature.

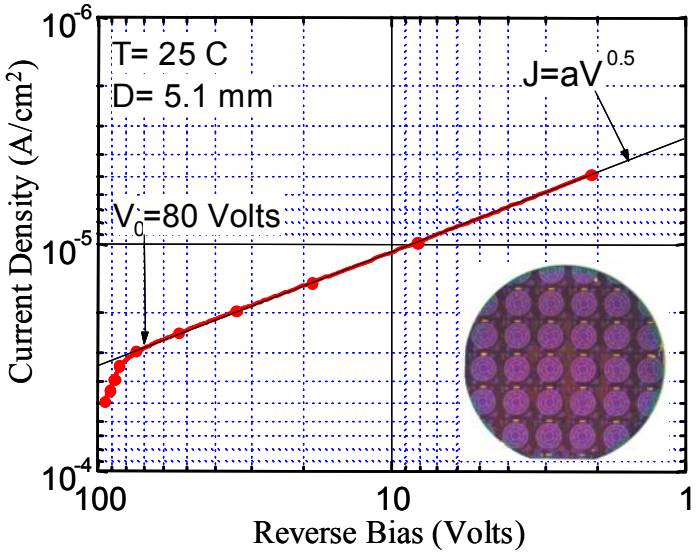

Figure 8. Current-voltage characteristic of a 5.1 mm modulator. Inset shows a fully processed 2-inch wafer.

Figure 9 shows the double-pass extinction ratio of a 5.1 mm device at different bias values. The extinction is more than 3 dB for 10 volts, which is similar to the extinction ratio of coupled-quantum well devices at 6 volts [16]. However, the thickness of this device is five times larger, and hence the capacitance is five times smaller. Since power consumption of a modulator at high frequencies is proportional to CV^2, where C is the device capacitance and V is the applied voltage, current device consumes almost half the power of coupled-quantum well devices. Also, the maximum extinction ratio of the modulator exceeds 12 dB, which is similar to the best-reported value for devices with an internal cavity. The absence of an internal cavity in this device however, provides an extremely wide field of

Downloaded From: https://www.spiedigitallibrary.org/conference-proceedings-of-spie on 14 Sep 2021
Terms of Use: https://www.spiedigitallibrary.org/terms-of-use

view that is crucial for mobile platform applications. In fact, this device has an improved extinction for beams coming at an angle, since their path-length is increased by $\sim(1\text{-}0.1\sin(\theta)^2)^{-1/2}$, where θ is the angle from normal.

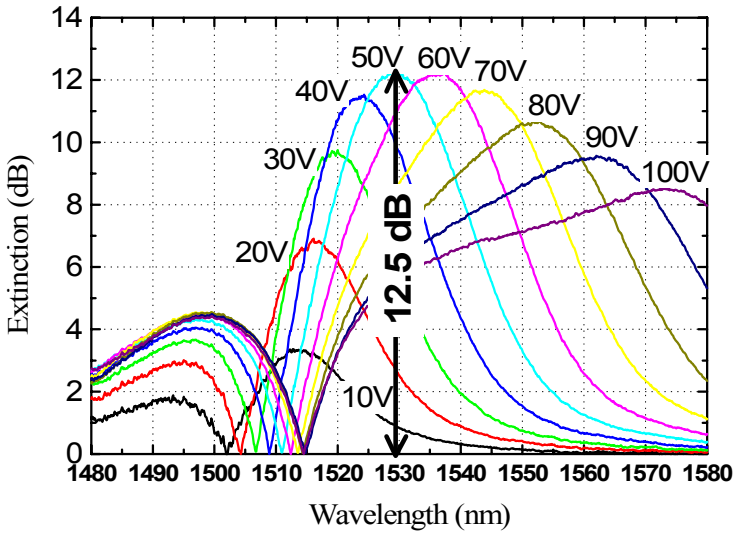

Figure 9. Measured double-pass extinction ratio spectra versus bias voltages from 0 to 100 volts.

More importantly, the optical bandwidth of the modulator is more than 60 nm for an extinction of 3 dB and signal level of 80 volts. Change of absorption edge versus temperature in this material is nearly 0.6 nm/°C, and hence applying a signal level of 80 volts ensures that the modulator has extinction above 3 dB over a 100°C range (see Figure 9). Since the power consumption increases with extinction ratio, it is logical to limit the extinction ratio to 2 to 3 dB for digital applications. We applied a signal level of 10 volts in addition to an adjustable DC bias.

Downloaded From: https://www.spiedigitallibrary.org/conference-proceedings-of-spie on 14 Sep 2021
Terms of Use: https://www.spiedigitallibrary.org/terms-of-use

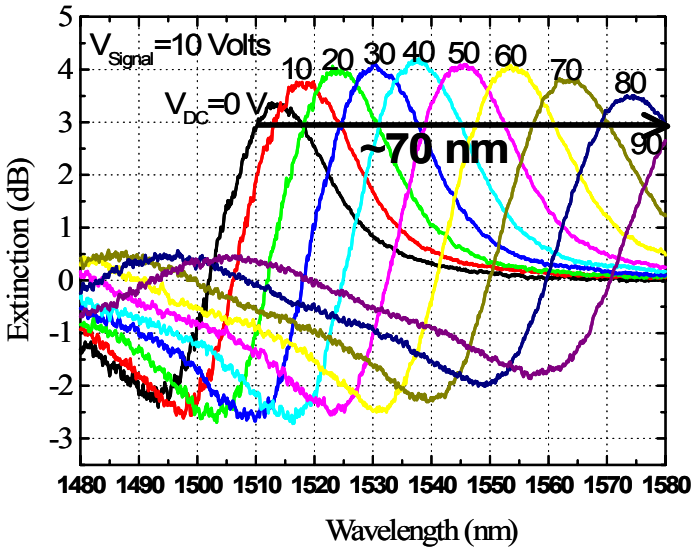

Figure 10. Measured double-pass extinction ratio spectra for a signal level of 10 volts and DC bias voltages from 0 to 90 volts.

The signal level is enough to produce an extinction ratio between 3.5 and 4.2 dB over the entire wavelength range, while a DC bias up to 90 volts could shift the peak modulation wavelength by about 70 nm (see Figure 10).

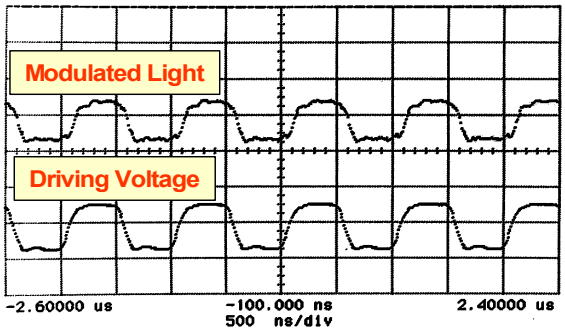

Figure 11. Single pass modulated optical signal for a 1 MHz square wave input signal.

The frequency response of the device was measured with a high voltage amplifier, and a fast infrared detector. Figure 11 shows the modulated optical signal for a square wave input signal at 1 MHz at λ~1550 nm. The large-signal performance is limited by the maximum current of the driver to about 200 nsec rise and fall times. However, small-signal 3 dB frequency bandwidth of the device exceeds 10 MHz.

VI. Conclusion

Downloaded From: https://www.spiedigitallibrary.org/conference-proceedings-of-spie on 14 Sep 2021
Terms of Use: https://www.spiedigitallibrary.org/terms-of-use

We have successfully modeled, fabricated, and tested different types of optical modulators based on our novel stepped quantum wells. These devices show superior performance compared with the rectangular quantum wells and even more sophisticated coupled quantum wells. The spatial separation of electrons and holes in the stepped quantum wells is believed to be the main reason for such performance. In particular, SQW phase modulators with nearly one order of magnitude higher efficiency, linearized modulators with more than two orders of magnitude higher linearity, and surface-normal modulators with nearly two times better efficiency and 7 dB higher extinction ratio compared with the conventional devices with rectangular and coupled-quantum well active layers are demonstrated.

VI. References

[1] F. Coppinger, A. S. Bhushan, and B. Jalali, "Photonic Time Stretch and Its Application to Analog-to-Digital Conversion," IEEE Trans. on Microwave Theory And Techniques **47**, 1309 (1999).

[2] E. Shekel, A. Feingold, Z. Fradkin, A. Geron, J. Levy, G. Matmaon, D. Major, E. Rafaely, M. Rudman, G. Tidhar, J. Vecht, and R. Ruschin, "64 x 64 Fast Optical Switching Module," Optical Fiber Communication Conference, Anaheim CA, OFC proceedings, 27 (2002).

[3] Y. Chan, and K. Tada, IEEE J. of Quantum Elect. **27**, 702 (1991).

[4] C. Thirstrup, IEEE J. of Quantum Elect. **31**, 988 (1995).

[5] H. Feng, J. Pang, M. Sugiyama, K. Tada, and Y. Nakano, IEEE J. of Quantum. Elec. **34**, 1197 (1998).

[6] H. Mohseni, H. An, Z. A. Shellenbarger, M. H. Kwakernaak, and J. H. Abeles, "Enhanced electro-optic effect in GaInAsP/InP three-step quantum wells," Applied Physics Letters **84**, p1823 (2004).

[7] H. Mohseni, H. An, Z. A. Shellenbarger, M. H. Kwakernaak, and J. H. Abeles, "Highly linear and efficient phase modulators based on GaInAsP-InP three-step quantum wells,"Applied Physics Letters **86**, p. 031103 (2005).

[8] H. Mohseni, W. K. Chan, H. An, A. Ulmer, and D. Capewell, "Tunable Surface-normal Modulators Operating near 1550 nm with a High Extinction Ratio at High Temperatures," IEEE Photonics Technology Letters **18**, p. 214 (2006).

[9] C. Thirstrup, IEEE J. of Quantum Elect. **31**, 988 (1995).

[10] J. Zucker, K. Jones, B. Miller, U. Koren, IEEE Photon. Tech. Lett. **2**, 32 (1990).

[11] See for example S. Hamilton, D. Yankelevich, A. Knoesen, R. Weverka, and R. Hill, IEEE Transactions on Microwave Theory and Techniques **47**, 1184 (1999).

[12] M. Kwakernaak, A. Lepore, H. Mohseni, H. An, Z. Shellenbarger, and J. Abeles, presented at Conference on Lasers and Electro Optics, Baltimore, MD, 2003 (unpublished).

[13] M. K. Chin, IEEE Photonics Tech. Lett. **4**, 583 (1992).

[14] S. Lee, R. Ramaswamy, V. Sundaram, "Analysis and Design of High-speed High-efficiency GaAs-AlGaAs Double-Heterostructure Waveguide Phase Modulators," IEEE J. of Quantum Elect. **27**, 726 (1991).

[15] G. C. Gilbreath, et.al., "Large Aperture Multiple Quantum Well Modulating Retroreflector for Free Space Optical Data Transfer on Unmanned Aerial Vehicles", Opt.Eng., **40** (7), pp. 1348-1356 (2001).

[16] H. Liu, C. C. Lin, and J. S. Harris, "High-speed, dual-function vertical cavity multiple quantum well modulators and photodetectors for optical interconnects," Opt. Eng. 40, 1186–1191 (2001).

[17] T. H. Stievater, W. S. Rabinovich, Peter G. Goetz, R. Mahon, and S. C. Binari, "A Surface-Normal Coupled-Quantum-Well Modulator at 1.55 Microns," IEEE Proceeding Conference on Lasers and Electro-optics CLEO'04, CThH3, San Francisco, California, May 2004.

[18] K. Ikossi , W.S. Rabinovich, D.S. Katzer, S.C. Binari, J. Mittereder, P.G. Goetz, "Multiple quantum well PIN optoelectronic devices and a method of restoring failed device characteristics," Microelectronics Reliability **42**, pp. 1021–1028, (2002).

Downloaded From: https://www.spiedigitallibrary.org/conference-proceedings-of-spie on 14 Sep 2021
Terms of Use: https://www.spiedigitallibrary.org/terms-of-use